Suppression of Necking in Polyethylene

A. P. Unwin,[1] R. A. Duckett,[1] I. M. Ward,[1] T. L. D. Collins,[2] J. Sweeney,[2] P. D. Coates[2]

[1]*IRC in Polymer Science and Technology, University of Leeds, Leeds LS2 9JT, United Kingdom*
[2]*Department of Mechanical and Medical Engineering/IRC in Polymer Science and Technology, University of Bradford, Bradford BD7 1DP, United Kingdom*

Received 1 October 2001; accepted 5 April 2002

ABSTRACT: The deformation behavior of a particular grade of high-density polyethylene prepared in a number of different ways has been examined. The samples all have an initially isotropic crystalline texture but differ in the levels of network preorientation surviving as a legacy of the melt processing history. Measurements of shrinkage and shrinkage force have been used to characterize this network, and the results suggest that the density of active chains is much lower than found in the main molecular network operating during solid-state drawing. The subnetwork properties vary depending on the level of extrusion and rate of cooling experienced during processing, with those entanglements surviving in the oriented melt at the point of crystallization having a long relaxation time. The presence of this subnetwork can lead to the suppression of necking during subsequent solid-state deformation. The implication is that simple processing procedures can be devised to remove or control the instability associated with necking. © 2002 Wiley Periodicals, Inc. J Appl Polym Sci 86: 3135–3147, 2002

Key words: polyethylene; necking; preorientation

INTRODUCTION

When subjected to large tensile strains, many polymers undergo necking, an instability characterized by a localized reduction in cross-sectional area. The phenomenon has been considered by many authors,[1–4] and it continues to provoke interest, not least in the processing field where there is a desire to control or avoid instabilities. In their studies, Coates and Ward[4] showed that the neck shape could be understood in terms of the strain hardening and strain rate sensitivity via the concept of a unique true stress– strain–true strain rate surface, and that homogeneous drawing was favored by higher levels of strain hardening. By studying a range of polyethylenes with differing morphologies, they were able to link the strain-hardening behavior and the strain rate sensitivity to the molecular weight and the morphology, respectively. In general, higher molecular weight produces a larger strain hardening at a given strain while slow cooled morphologies produce a larger strain rate sensitivity. These findings offered the prospect of controlling and even eliminating the necking instability.

The strain-hardening feature of stress–strain curves is often modeled using the concept of a deforming molecular network. The classical rubber elasticity model was developed for chemically crosslinked materials that showed large strain elastic behavior,[5] but the concept of a continuous deforming network underpinning the deformation process has been extended to noncrosslinked materials.[6] The almost complete recovery shown by many oriented polymers, when taken a little above the glass transition or crystalline melting temperatures, provides strong justification for this approach. The main modification to the classical rubber theory has been the incorporation of slip links[7,8] with a temperature-dependent mobility to model the physical molecular entanglements present in thermoplastic polymers. These later models have been used successfully to explain the deformation behavior of noncrosslinked materials[9] and now form the physical basis underpinning many attempts to model deformation behavior.[10,11]

This article reports investigations into the deformation behavior of a commercially available polyethylene in which the necking instability can be removed. Measurements of shrinkage and shrinkage stress in precursor processed sheets are combined to investigate the nature of the molecular network, and the impact for the strain-hardening and subsequent deformation behavior is considered in the light of these results. The results suggest that the control of some extrinsic variables can lead to modification of the strain-hardening behavior and suppression of the necking instability. This is quite important, particularly as the main parameter controlling strain hardening, the molecular weight, is an intrinsic variable.

EXPERIMENT

Materials

A single grade of polymer, namely a branched high-density polyethylene (HM4560, B.P. Chemicals, with

Correspondence to: I. M. Ward (i.m.ward@leeds.ac.uk).

Journal of Applied Polymer Science, Vol. 86, 3135–3147 (2002)

molecular weight characteristics, $\bar{M}_w$ ~225,000 and $\bar{M}_n$ ~24,000) has been investigated here. The branch content is, on average, less than 1.5 butyl branches per 1000 carbon atoms. Commercially, it is available in oriented products (containing about 2.5% by weight carbon black to give a degree of UV protection) for use as a reinforcement in civil engineering and landscaping applications from Netlon. This article reports investigations performed on the processed sheet, which forms the precursor to the oriented commercially available products. The precursor sheets are available in three thicknesses, namely 2.8, 3.9, and 6.0 mm, and are made by melt extrusion using a machine of single screw design, operating at a melt temperature of 190°C. The 8 mm-thick output from the extruder is reduced to a thickness close to that of the final precursor sheet by flow through a converging die, and then passed between rollers to a cooling stage. The degree of deformation is therefore greater for the thinner precursor sheets.

For the detailed investigations reported here, thin layers from the surface (S) and the middle (M) of the precursor sheets were obtained by machining away surplus material. Layer thicknesses were typically ~0.4 mm, although additional middle layers of 1-mm thickness were also produced for more accurate work. For comparison, isotropic sheets of this polymer without the carbon black filler were obtained by compression molding pellets at 160°C in a hot press. After 10 min in the press the sheet was cooled by either removing the mold from the platens and immersing it in cold water (*Q*) or by leaving it *in situ* and passing moist air through the platens (SC). These samples will be referred to as W4560 to distinguish them from those obtained from the processed precursor sheets, P4560.

Characterization

Differential scanning calorimetry

Specimen melting behavior was investigated at a heating rate of 10 K min^{-1} using a Perkin-Elmer differential scanning calorimeter, DSC7, calibrated using an indium standard. Crystallinity values were calculated from the area under the melting endotherm and using a value of 290 J g^{-1} for ΔH, the heat of fusion of the orthorhombic crystal.

X-ray diffraction

The crystalline texture was examined by exposing samples to a fine X-ray beam, incident normally to the sheet surface and detecting the scattered radiation using photographic film. Tests were performed on surface and central layers of all three precursor sheets and on the compression-molded sheets. Several pole figure analyses were performed on selected samples to reinforce conclusions obtained from photography.

Shrinkage and shrinkage force

Free shrinkage experiments were performed in silicone oil at 160°C to assess the level of preorientation in the precursor sheets. Rectangular specimens 60 mm (along the sheet extrusion direction) × 5 mm were cut and marked at regular intervals before being placed in a small wire cage with a wire lid. The purpose of the cage was to keep the sample straight during shrinkage yet reduce contact with the sample so that frictional forces could be minimized. Samples were allowed to shrink freely for 30 min before being removed from the oil bath. The separation of the markers and dimensional changes were measured after shrinkage.

Measurements of shrinkage force along the extrusion direction of the precursor sheets were performed using equipment described elsewhere[12] in a silicone oil bath at a temperature of 160°C. Samples of length 60 mm and about 5 mm wide were mounted between two clamps—one fixed and one attached via a cantilever arm to a LVDT transducer. A small preload was applied to the sample before it was immersed in the oil bath. The rise and decay of the shrinkage force was monitored over a period of 20 min using a data logger and the shrinkage stress variation over this period of time calculated using the cross sectional area at the start of the test.

Drawing behavior

The uniaxial tensile drawing behavior was examined at a constant true strain rate of 0.005 s^{-1} and a temperature of 100°C using an Instron tensile testing machine. During the test, the crosshead speed was increased so as to maintain a constant strain rate based on the changing separation of the clamps. This equates to the local strain rate in the sample for homogeneous deformation between the clamps. End effects and necking would tend to produce deviations from this. The samples were monitored for necking behavior during deformation and several tests were stopped at intermittent strains to check this in more detail. For P4560 samples, drawing tests were performed both parallel to (0° inclination) and perpendicular to (90° inclination) the extrusion direction of the sheet.

RESULTS

Differential scanning calorimetry

The melting behavior of layers of thickness 0.05 mm cut from the center and the surface of the precursor sheets is shown in Figures 1 and 2. For comparison,

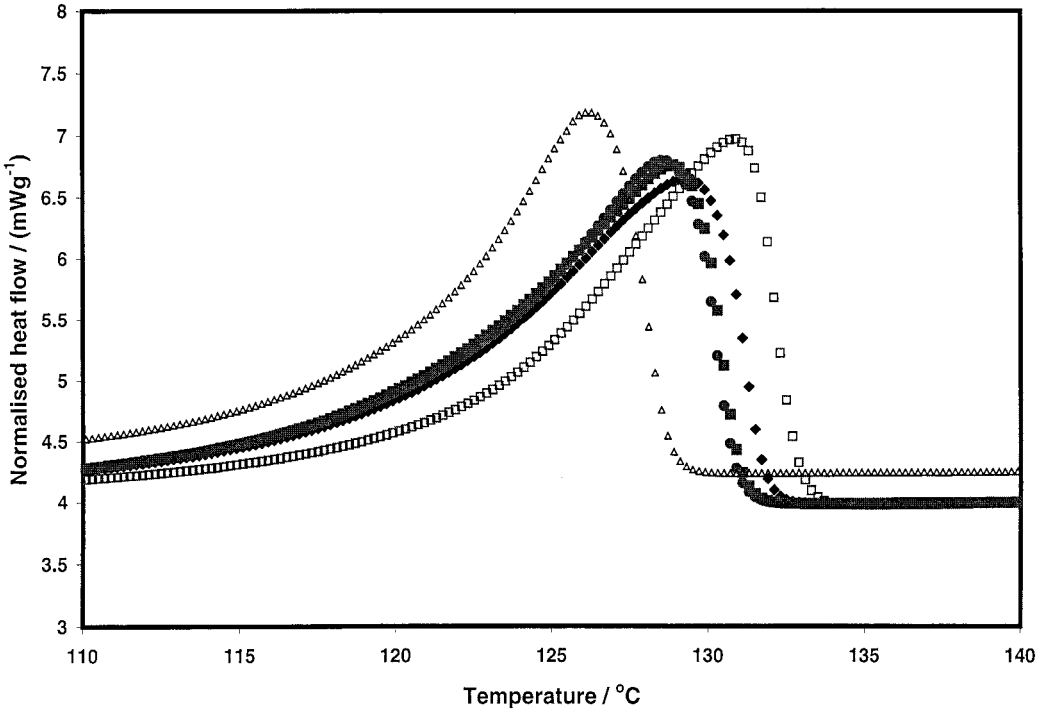

Figure 1 Melting endotherms for central sections of precursor sheet (P4560) of thickness ●, 2.8 mm ■, 3.9 mm; and ◆, 6.0 mm and compression-molded sheet (W4560) □, slow-cooled and △, quenched.

results for the compression-molded material are also shown. For central sections of P4560 there is very little difference in the melting behavior of the different sheets. The melting behavior is found to be intermediate between that for quenched and slow-cooled samples of W4560 compression-molded sheet. In contrast, the surface sections of P4560 show some variation between sheets. Generally, the melting peak occurs at a slightly lower temperature than seen in the central sections, and more closely approaches that of the

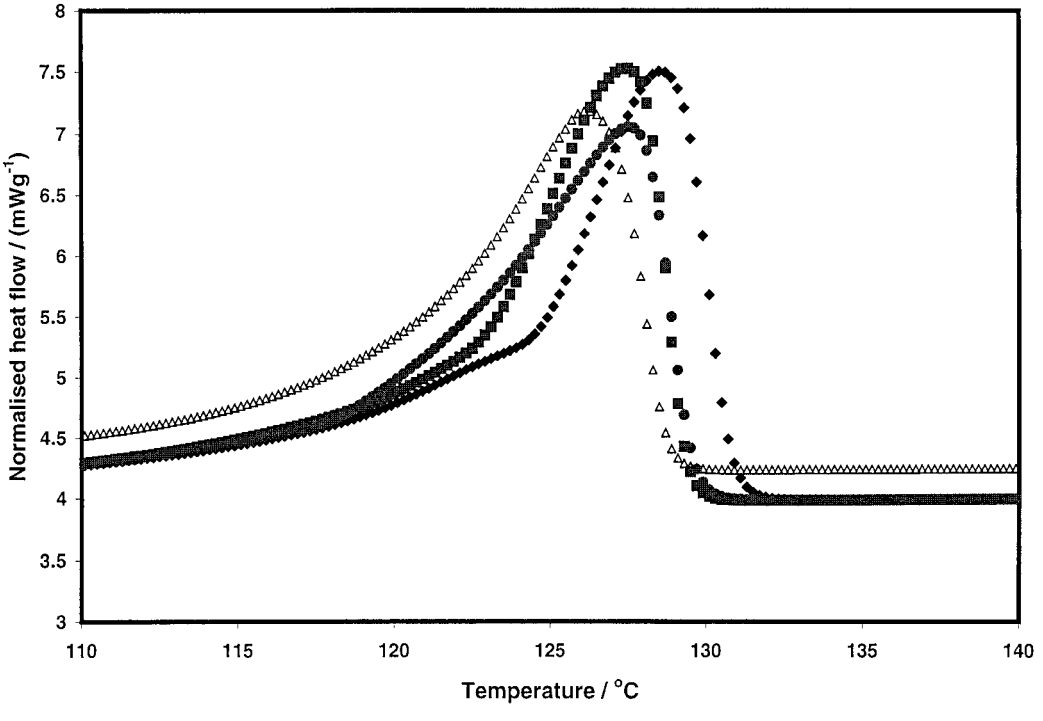

Figure 2 Melting endotherms for surface sections of netlon precursor sheet (P4560). Key as for Figure 1.

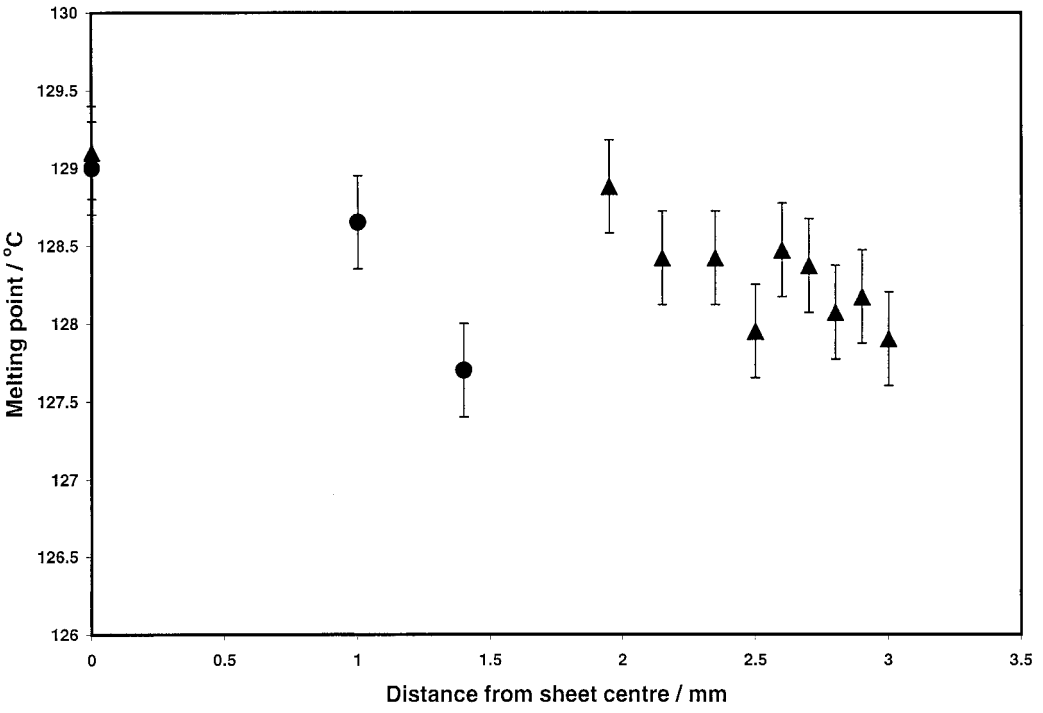

Figure 3 Variation in peak melting point of sections of precursor sheet (P4560) as a function of distance from sheet center. Sheet thickness ●, 2.8 mm and ▲, 6.0 mm.

quenched compression-molded sheet. There is also evidence of a low temperature shoulder possibly arising from the melting of material at the outermost surface section where contact occurred with the cooling rollers.

Figure 3 shows the variation in melting point with position in two of the precursor P4560 sheets. In this case results for the surface and center layers are the averages of multiple measurements. It is easier now to make out trends in the melting point. There is little difference in the melting points at the center of the sheets but towards the surface the melting point falls slightly, indicating the presence of smaller crystals formed at higher levels of supercooling. This is to be expected because, during crystallization, the surface zone should be cooler than the bulk of the material due to contact with the cooling rollers and the ambient environment. The shoulder seen in Figure 2 is confined to the outer-most layer, suggesting a narrow chill zone. Results of crystallinity and melting point for surface and central sections of the three precursor sheets are given in Table I.

X-ray diffraction

Analysis of X-ray diffraction measurements on samples of the precursor sheet showed no indication of any preferred crystalline orientation. Photographs showed isotropic diffraction rings with no observable variation in intensity with azimuthal angle. The crystalline texture is isotropic within the limits of experimental error, and this was confirmed in several pole figure scans that are not limited to the two-dimensional investigations afforded by the photographic approach.

TABLE I
Characterisation of Layers from Processed Precursor P4560 Sheet

Sample	Crystallinity/ %	Peak m.p./°C	Residual draw ratio, λ_{res} from shrinkage	Shrinkage stress/kPa	Number of active chains per unit volume/10^{23} m^{-3}	λ_{pro} from stress–strain curve matching	Subnetwork stress/MPa
6 mm—S	52.5	127.9	2.8	12	2.7	1.06	0.39
3.9 mm—S	52.0	127.5	2.95	30	6.0	(1.11–1.16)	0.97
2.8 mm—S	51.1	127.6	3.15	38	6.6	(1.11–1.16)	1.2
6 mm—M	53.4	129.1	2.45	14.5	4.3	1.06	0.48
3.9 mm—M	53.0	128.9	3.5	22	3.1	1.14	0.7
2.8 mm—M	52.6	129.0	4.55	29.1	2.4	1.22	0.92

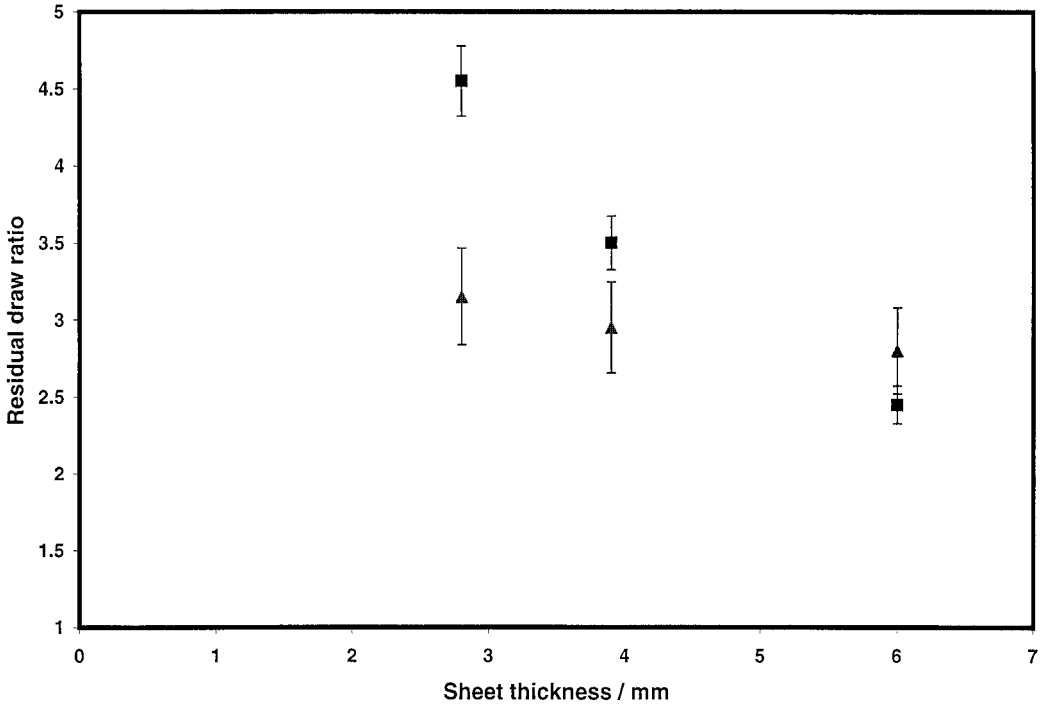

Figure 4 Residual draw ratio (or effective network draw ratio) evaluated from free shrinkage measurements as a function of thickness in processed Netlon sheet (P4560); ■, center layer, ▲, surface layer.

Shrinkage and shrinkage stress

Annealing at 160°C caused initially rectangular precursor sheet samples to shrink along the direction of extrusion. Essentially, the shapes remained rectangular with an expansion in dimension perpendicular to the extrusion direction accompanying the shrinkage. Measurements from both the specimen dimensions and the regular lines marked on the sample indicated a high degree of homogeneity, although a degree of curvature in some annealed samples indicated that local variations in the shrinkage existed. Results of free shrinkage measurements on the processed precursor sheet are shown in Figure 4 and listed in Table I. The data are presented in terms of the precursor residual draw ratio for the extrusion direction, defined as the ratio of the initial length to the length after shrinkage is complete. Clearly, the processed sheet has a significant residual frozen-in draw ratio originating from the production process, and this varies between sheets as well as within sheets. It is also apparent that the levels of residual strain are greater than that expected solely on the basis of passage through the convergent die, which would only impose a draw ratio of about 1.3 on the 6-mm sheet.

Figure 5 shows the variation in shrinkage stress with time at 160°C in a sample cut from the central section of the 2.8-mm precursor P4560 sheet. Free shrinkage measurements indicated that this sample has a residual draw ratio of about 4.5. Figure 6 shows results obtained from a sample of W4560-Q sheet that had been drawn to a draw ratio of approximately 4 at 100°C. In this case, the shrinkage stress was measured at a temperature of 150°C because tests at the higher temperature caused the sample to rupture preventing accurate measurement of the peak stress. The peak stress developed in the processed material is about 35 kPa, and it decays gradually over a period of about 1500 s. In contrast, the shrinkage stress in the material drawn to a similar draw ratio at the lower temperature is considerably greater, 8 MPa, and it decays much more rapidly. The rate of decay slows at longer times, and no measurable change is detected beyond 20 s. It is still possible, however, that small changes, comparable to those seen in the processed material and beyond the resolution of Figure 6, are still occurring. Table I displays the peak shrinkage stress values in the precursor sheets. For the central sections the values quoted are the average of four tests.

For a uniaxial deformation, λ, classical rubber elasticity theory can be used to relate the peak shrinkage stress and the shrinkage using the equation

$$t = NkT\left(\lambda^2 - \frac{1}{\lambda}\right)$$

where t is the true stress and λ is the extension ratio derived from the free shrinkage measurements assuming that the network has recovered completely. The remaining parameters are the Boltzmann constant, k, the absolute temperature, T, and the classical entan-

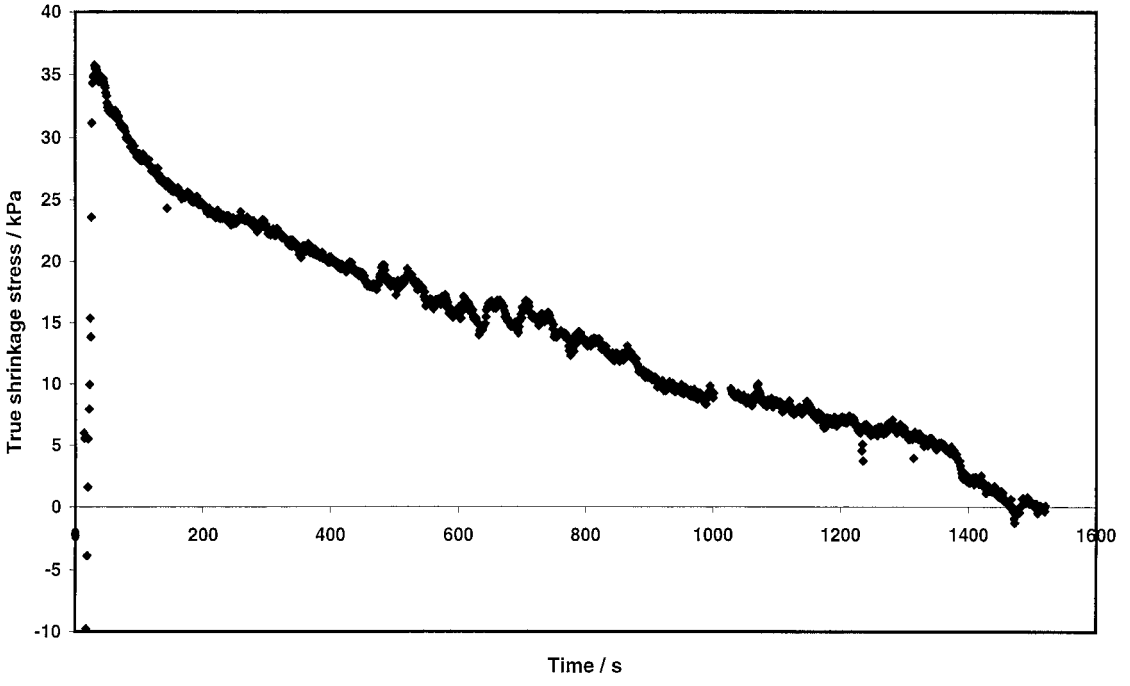

Figure 5 Variation in shrinkage stress with time in a central section of 2.8 mm processed Netlon sheet (P4560).

glement density, N, which characterizes the network. This equation, incorporating the residual draw ratio from shrinkage measurements, has been used to characterize the network present in the precursor material. Table I lists the entanglement densities for the different precursor P4560 sheets. For comparison, a value of 8.7×10^{25} active junctions is obtained from the sample considered in Figure 6. This is more than two orders of magnitude higher than the values found in the precursor sheets. The values associated with the precursor sheets reflect a very loose network, very different from that characterizing the material drawn at 100°C.

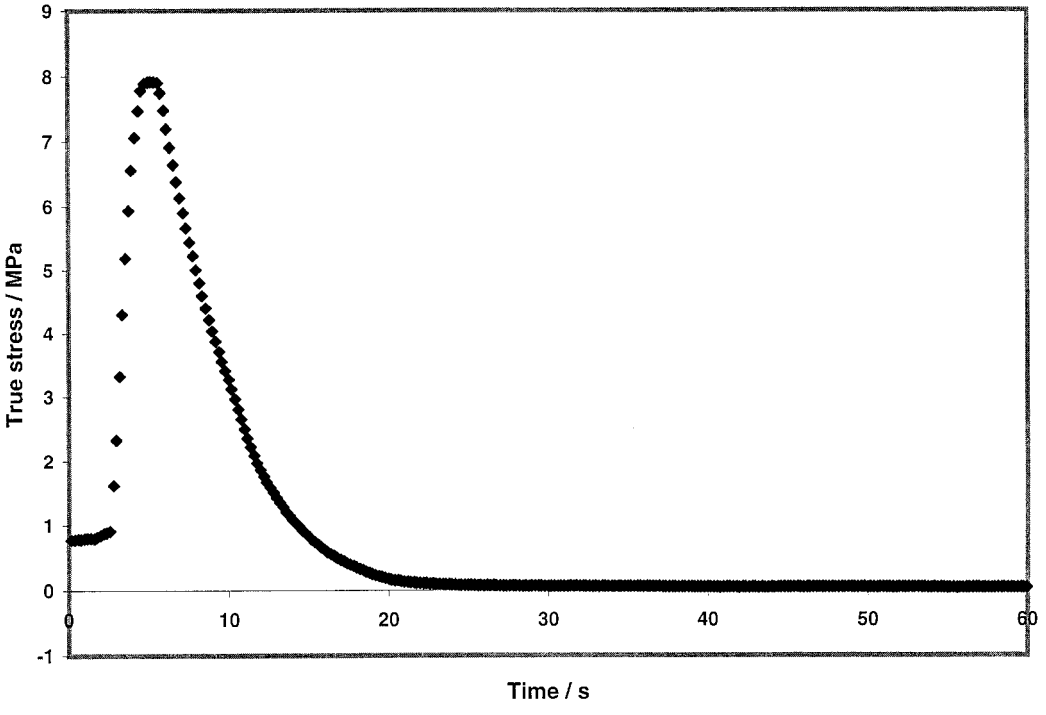

Figure 6 Variation in shrinkage stress with time in unfilled compression-molded W4560 sheet, drawn to a draw ratio of approximately 4 at 100°C.

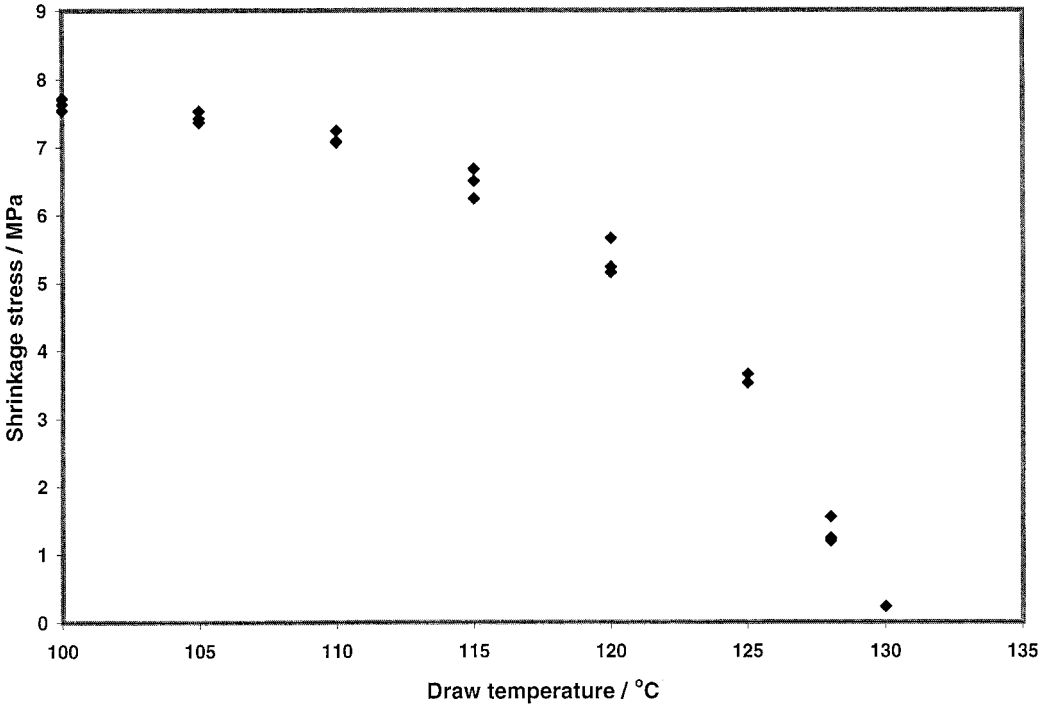

Figure 7 Variation of true shrinkage stress in oriented unfilled compression-molded W4560 sheet with draw temperature.

The sheets were extruded at approximately constant width, so strictly the shrinkage stress/draw ratio relationship is

$$NkT\left(\lambda^2 - \frac{1}{\lambda^2}\right).$$

The shrinkage stress measurements, however, were not conducted under conditions where constant width was rigorously maintained, so the network measurements can only be regarded as semiquantitative.

Clearly, the entanglements present in this polyethylene are not permanent as in a crosslinked rubber network nor stable in the sense shown by PET when processed over a range of temperatures. It is more realistic to envisage the entanglements as slip links whose mobility increases with temperature so that the various relaxation processes can operate to relieve the entropic stresses.

This interpretation is reinforced by more detailed measurements of shrinkage stress, performed on compression-molded W4560-Q sheet drawn over a range of temperatures between 100 and 130°C to the same nominal draw ratio of 4. Figure 7 illustrates how the peak shrinkage stress in these samples varies with the drawing temperature. The measured draw ratio of drawn samples varied by as much as 5% from the nominal draw ratio so the data has been corrected for a common draw ratio of 4 to allow comparison. This experiment shows that the effective stress arising from entanglements falls when drawing is performed at higher temperatures and, because the recovery is unaffected by the drawing temperature, Figure 7 illustrates that the density of entanglements falls as the draw temperature is increased. The greater opportunity for relaxation in the precursor sheets, associated with the much higher processing temperature and the finite cooling time, accounts for the much looser network. To avoid confusion, this loose network present in the precursor sheets will subsequently be referred to as a subnetwork.

Drawing behavior

Uniaxial testing revealed a considerable difference in deformation behavior between samples of this single grade of material. All compression-molded W4560 samples and all precursor P4560 samples drawn perpendicular to the extrusion direction showed necking. Generally, the precursor samples drawn parallel to the extrusion direction deformed homogeneously, although samples of the central section of the 6 mm-thick sheet appeared to show a shallow neck.

These differences in deformation behavior are accompanied by differences in the development of flow stress with strain. Figures 8 and 9 illustrate the differences that can exist within the 2.8 mm-thick precursor sheet. In Figure 8, the anisotropy in the development of nominal flow stress with draw ratio is shown for layers cut from the center of the sheet. Both samples were drawn at a true strain rate of 0.005 s^{-1} at 100°C. When drawn parallel to the extrusion direction, the

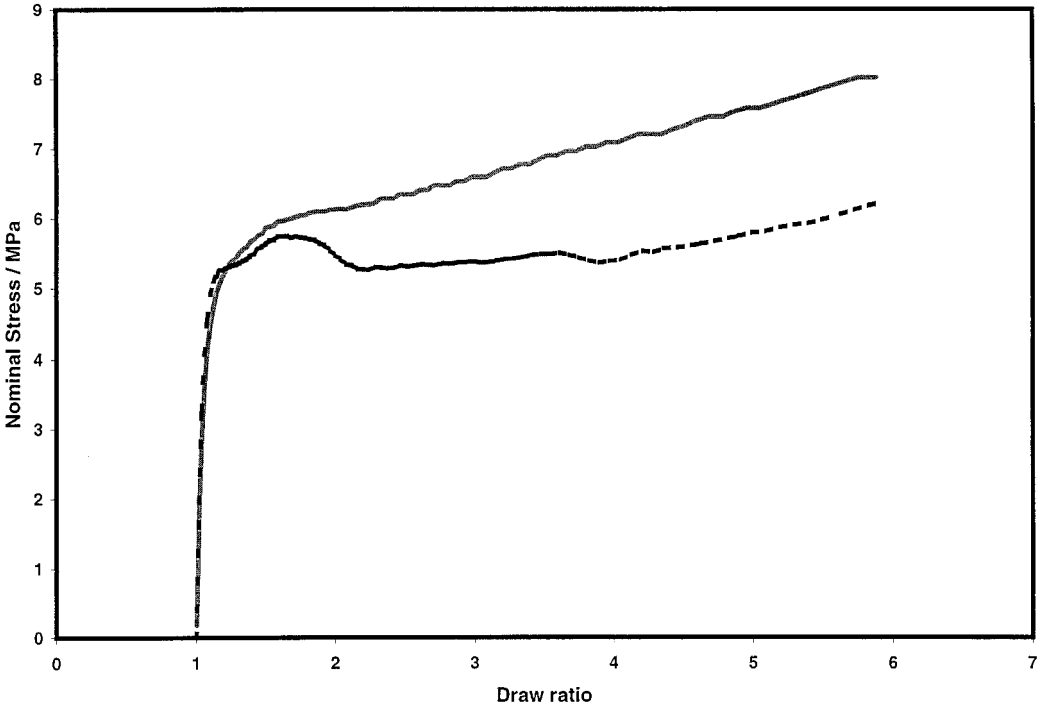

Figure 8 The development of the nominal drawing stress in processed 2.8 mm-thick precursor sheet with draw ratio at 100°C and a true strain rate 0.005 s^{-1}. Tensile drawing was either parallel to (0° inclination), —, or perpendicular to (90° inclination), - - - - -, the extrusion direction of the sheet.

material shows a monotonically increasing nominal flow stress and no indication of inhomogeneous deformation. When drawn perpendicular to the extrusion direction, however, a peak in the curve occurs at low strains where necking is observed. Necking is complete by a draw ratio of about 4, so the homoge-

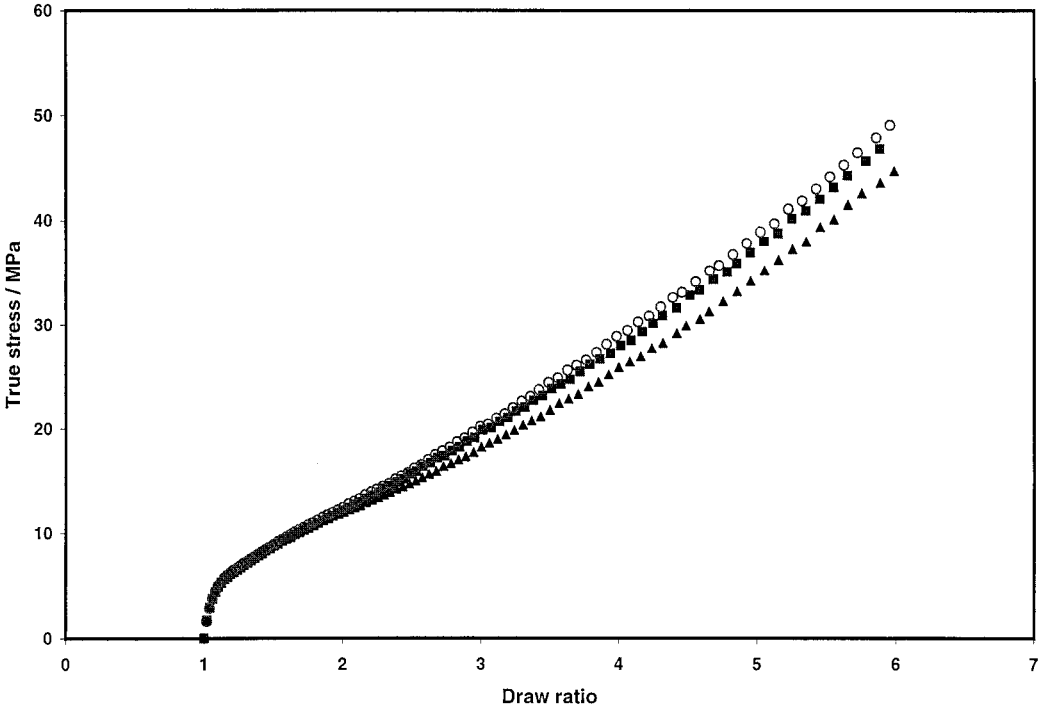

Figure 9 True drawing stress parallel to (0° inclination) the extrusion direction in processed 2.8 mm-thick precursor sheet at 100°C and a true strain rate 0.005 s^{-1} as a function of draw ratio for different sheet sections; ▲, surface; ■, 0.4 mm depth; and ○, middle.

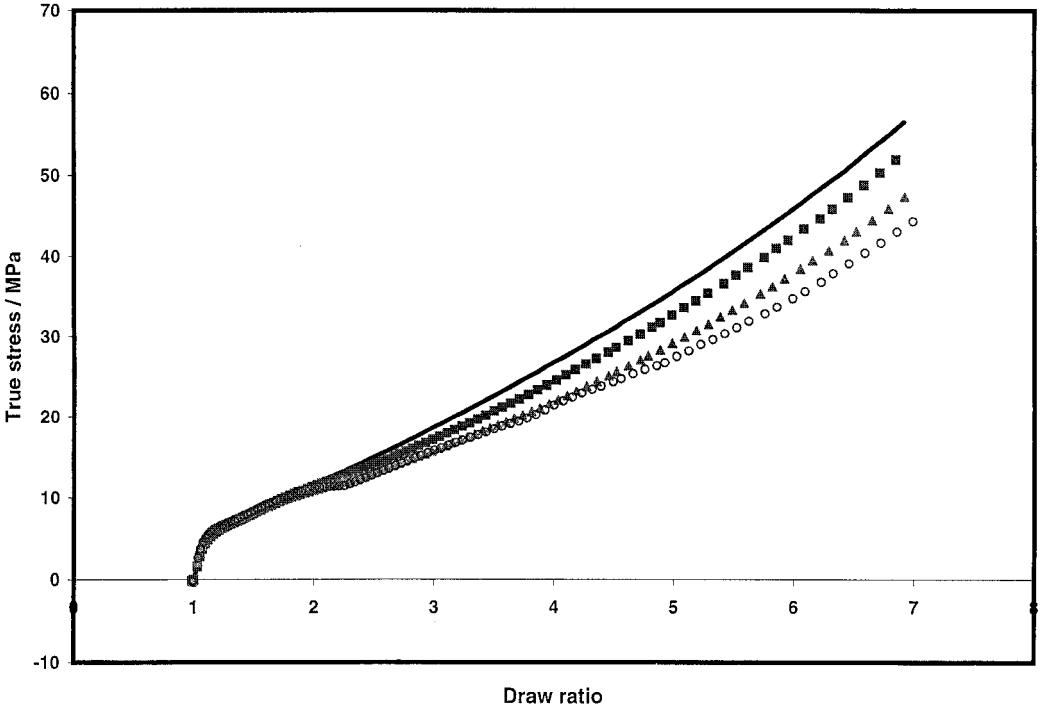

Figure 10 True drawing stress of center sections of precursor sheet as a function of draw ratio for drawing parallel to the extrusion direction. All samples were drawn at a true strain rate 0.005 s^{-1} at 100°C. Precursor sheet thickness, —, 2.8 mm; ■, 3.9 mm; and ▲, 6 mm. Reference curve; ○, data for drawing of 6 mm-thick sheet perpendicular to the extrusion section. Sections of the curves for the 6-mm sheet, where the true stress is indeterminate because of inhomogeneous drawing, are omitted.

neous deformation occurring in both samples at a draw ratio of 6 requires very different stress levels depending on the inclination of the drawing direction to the extrusion direction.

Figure 9 illustrates differences occurring across the profile of the same 2.8 mm-thick precursor sheet. These samples have been drawn parallel to the extrusion direction under the same conditions described above. The homogeneous deformation of these samples enables the results to be presented in the more useful form of the true drawing stress. The results indicate that the true drawing stress develops more slowly in layers closer to the sheet surface, although the differences are minimal beyond a depth of 0.4 mm from the surface.

Some limited tests were performed on samples of precursor P4560 sheet in which constrained annealing had been performed to allow relaxation of the molecular network. These samples were obtained by annealing 0.35 mm-thick sections (cut from the center of the 2.8 mm-thick precursor sheet) at 160°C under a low compressive force between steel plates for 90 min, followed by subsequent quenching into water at room temperature. The samples did not shrink during annealing and free shrinkage tests after annealing indicated no residual draw ratio, suggesting that the molecular network had completely relaxed. The drawing behavior of the annealed sample was compared with that of compression-molded W4560-Q material. The melting behavior of both these samples indicates that they have similar morphologies so that the only difference between them is the presence of the carbon filler in the processed precursor material. The drawing behavior of these samples was indistinguishable (similar to that shown in Fig. 8 for the perpendicular drawing) confirming that relaxation of the molecular network removes the anisotropy in the precursor material, and that the carbon filler has a negligible effect on the drawing behavior, when similar morphologies are prepared.

The effect of morphology was considered in tests on the compression-molded sheets prepared by slow and quench cooling. It was found that the morphology only affects the initial yield stress, with W4560-SC samples showing a greater yield stress than quenched samples. Otherwise, both samples show necking and similar development of drawing stress at high strain.

Figure 10 shows the true stress–strain curves for the central sections of the different precursor sheets for drawing parallel to the extrusion direction. With the exception of the 6 mm-thick sheet, which shows a very shallow neck, these samples deform homogeneously. Clearly, the drawing behavior depends on the initial sheet thickness. In contrast, drawing perpendicular to the extrusion direction reveals no differences in terms of either necking or development of drawing stress,

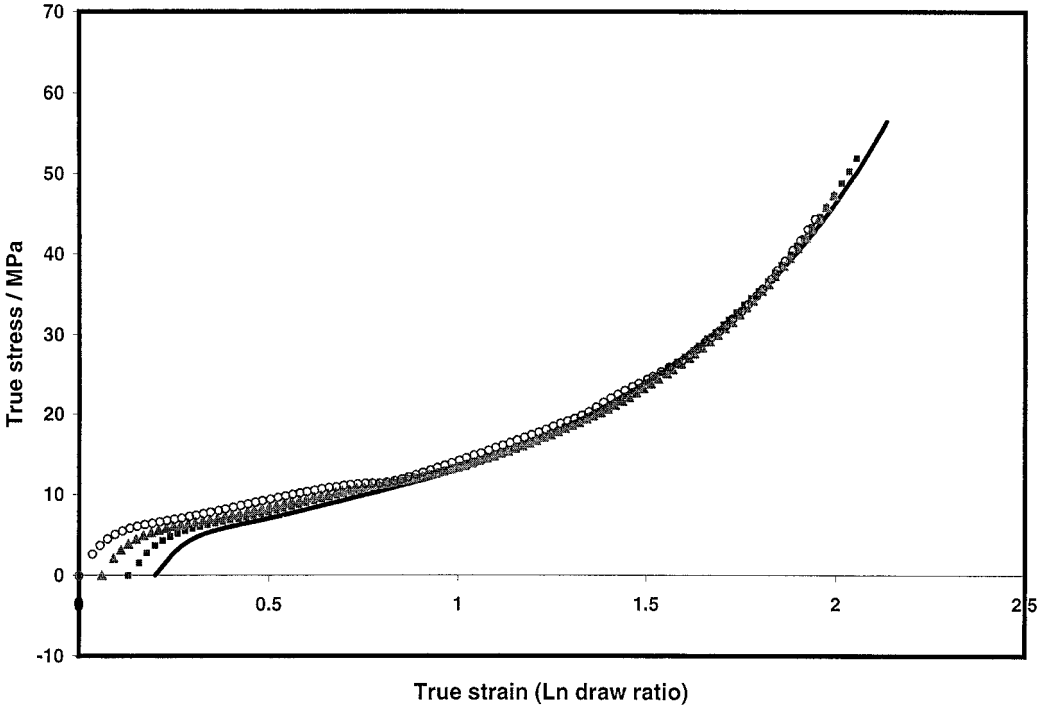

Figure 11 Transposed true stress–strain curves (from Fig. 10) for centers of processed netlon sheet. All curves are shifted to give coincidence with the strain-hardening behavior of the reference curve. Key as for Figure 10

and the behavior is indistinguishable from that of the quenched compression-molded material. For comparison, the results for the 6 mm-thick sheet are also shown in Figure 10.

DISCUSSION

There are significant differences in the drawing behavior of nominally isotropic samples of this particular grade of polyethylene relating to the processing history. The precursor sheets show anisotropic drawing behavior, the exact nature of which depends on the position within and the thickness of the sheet. Of particular interest is the suppression of the necking instability in some samples. The anisotropy and comparisons with control samples have confirmed that neither the filler nor the crystalline morphology are responsible for this behavior. Instead, the observation of shrinkage in the precursor sheets appears to be linked to the suppression of the necking instability, and it is particularly striking that the instability returns when the shrinkage is removed by constrained annealing.

The concept of stress–strain curve matching[13] has been used to interpret the behavior of polymers that display levels of molecular orientation (e.g., arising from high wind-up speeds during processing) prior to drawing. By applying this procedure to polyethylene terephthalate, Long and Ward[14] showed that the properties of pin-drawn fibers could be understood by combining the deformations imposed during the two steps of the processing. This implied the existence of a continuous network (i.e., one with stable junction points) underpinning the deformation process, although it was recognized that variations in the drawing process, such as embodied in pin and plate drawing, could introduce modifications to the network.

Figure 11 applies this concept to the stress–strain curves shown in Figure 10. All curves are shifted along the natural strain axis to give coincidence with the strain-hardening behavior of the reference curve, taken to be that of the fully relaxed material. The strain axis shift values can then be converted to the equivalent network draw ratios, λ_{pro}, introduced into the precursor sheets during processing. These results are compared in Table I with values for the residual draw ratios, λ_{res}, obtained from the shrinkage measurements. Although the curve matching produced by transposition is very good, the lack of agreement between λ_{res} and λ_{pro} means that it is incorrect to interpret the behavior in terms of a continuous deforming network.

It is more appropriate, therefore, to consider that the network is maintained by junction points with limited stability. Figure 7 shows that the stability of these junction points decreases at higher temperatures, but other factors such as the level of deformation may also have an impact. This is suggested by consideration of the different subnetworks in precursor samples where it is found that the entanglement density is not con-

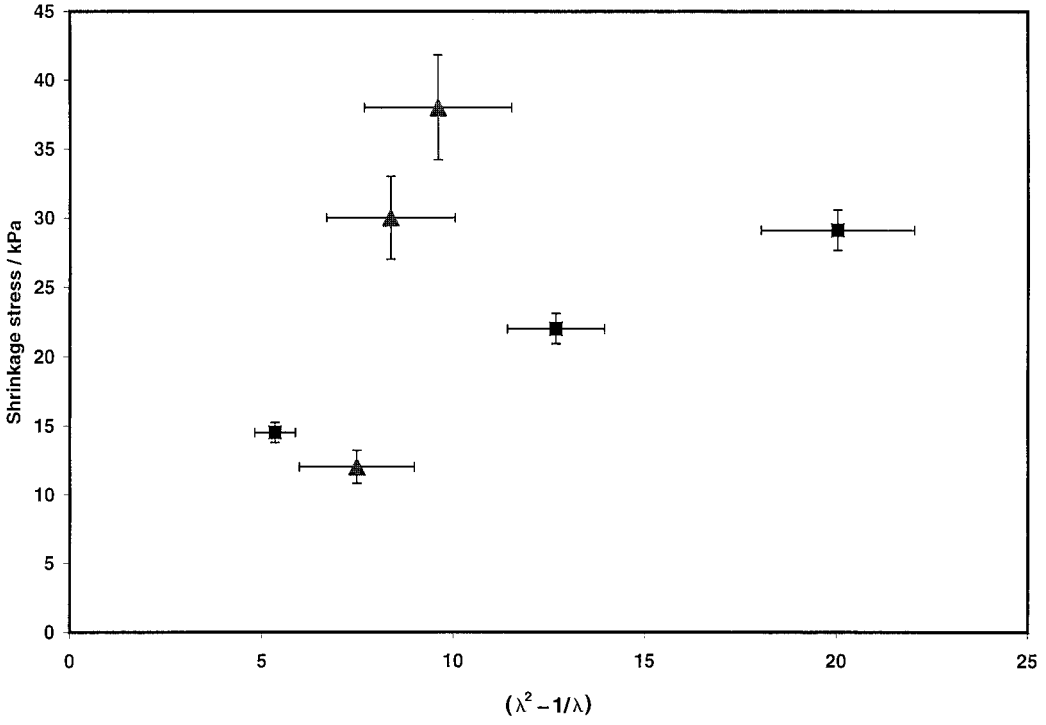

Figure 12 Variation in shrinkage stress with $(\lambda^2 - 1/\lambda)$ for samples obtained from precursor sheet (P4560); ■, center layer, ▲, surface layer.

stant in samples processed at the same temperature. Figure 12 plots the shrinkage stress against

$$\left(\lambda_{res}^2 - \frac{1}{\lambda_{res}}\right)$$

for the different precursor samples. The classical rubber elasticity theory predicts that these would lie on a common straight line if there were a common "precursor network." The particular strain and thermal histories followed by material elements of the precursor sheets during processing will depend on the final sheet thickness and the location within the sheet. These unknown different histories, coupled with a probable complex spectrum of relaxation times for the entanglements, makes it difficult to reach concrete conclusions, especially in the case of surface sections where the thermal history in particular is uncertain. For central sections there are likely to be less severe temperature gradients, and it is reasonable to conclude that the thermal histories are relatively similar. The good agreement in the melting points of these samples supports this view. Values for the number of chains/unit volume for the central layers of precursor sheet show that the thicker sheets have retained a greater density of junction points, despite the probable longer exposure to high temperatures arising from the longer cooling times associated with thicker sheets. It appears that the higher strains associated with the thinner sheets have promoted faster relaxation as has been observed by Osaki et al.[15]

Clearly, however, the precursor subnetwork has an influence on the drawing stress, and it is proposed that there are two interpenetrating networks acting in parallel, only one of which, the subnetwork, is retained at high temperature owing to the greater stability of its entanglements. Both contribute to the low temperature deformation. The characteristics of the high-temperature subnetwork can be probed by the shrinkage and shrinkage force measurements of the precursor sheet, because the dominant isotropic network is effectively invisible due to the low stability of its junction points. At lower temperatures, where both networks are relatively stable, it is possible to consider the contributions to the development of stress with strain separately.

This is done in Figure 13, which shows the development of stress at 100°C in two Gaussian networks with differing characteristics as a function of the imposed strain. The upper curve considers the deformation of the initially isotropic (fully relaxed) network with characteristics determined from the sample considered in Figure 6. The lower curve is the further deformation of the high temperature subnetwork from an initial deformation ratio of 3. The strain in the subnetwork is obtained by combining the residual and imposed strains so that at an imposed draw ratio of 6 the subnetwork draw ratio is about 18. The levels of

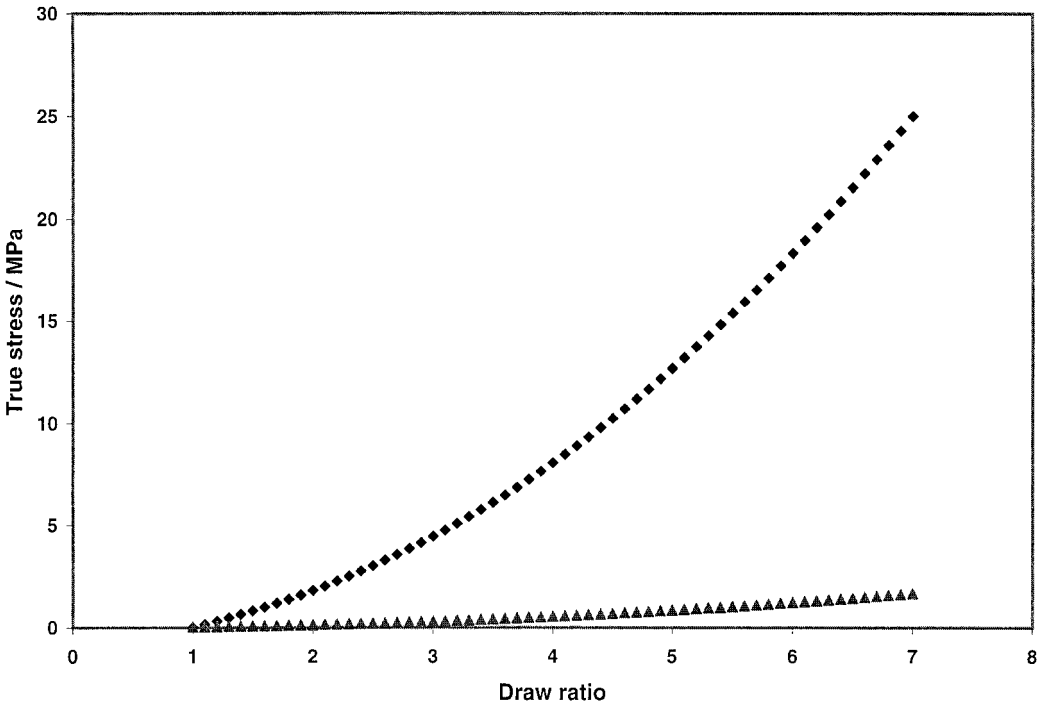

Figure 13 The development of network stress in two Gaussian networks with characteristics derived from shrinkage measurements of precursor P4560 sheet, ▲, and oriented W4560, ◆.

strain are very high but still considerably less than the model limits suggested by the very low density of active chains.

The stress contributions from these two networks at a common imposed draw ratio of 6 (different real draw ratios) are 1.2 MPa for the subnetwork and 19 MPa for the dominant main network. So the subnetwork contributes a stress about 6% of that in the main network. For comparison, the stresses developed in the samples of the relaxed W4560 and the precursor 2.8-mm sheet at an imposed draw ratio of 6 and a draw temperature of 100°C are 35 and 46 MPa, respectively. So, if it is assumed that the difference between the two samples is the presence of an additional precursor subnetwork in the 2.8-mm sheet, it can be seen that this "precursor network" produces an additional stress of 11 MPa, or a bit more than 30%, in practice.

It is not intended to suggest that the rubber elasticity model describes adequately the strain-hardening behavior of this polyethylene. The same effect can possibly be explained by more realistic models[7]such as the Edwards and Vilgis model where additional strain hardening can be introduced by increasing the inextensibility parameter, α. More importantly, the drawing temperature of 100°C is below the crystal melting point so other contributions would certainly need to be considered, not least modifications to the characteristics of the networks and considerations on whether the chains can fully explore conformational space. However, in the absence of sufficient information to permit the use of such models, Figure 13 suggests that the concept of a deforming subnetwork in parallel with the main network can explain the differences in the levels of strain hardening seen in the differently prepared samples of this grade of polyethylene. Parallel work on mathematical modeling of the large strain deformation of this material[16] has confirmed that the incorporation of a Gaussian subnetwork acting in parallel with a viscoelastic network model does predict the observed behavior quite well.

The Gaussian subnetwork stresses at an imposed draw ratio of 6 and a temperature of 100°C for the different precursor sheets are given in Table I. Figure 14 shows that these correlate reasonably well with the shift factors found in stress–strain curve matching, in the sense that the larger stress contribution comes from those samples that require the larger shift in stress–strain curve matching.

The effect of an additional subnetwork stress contribution on the necking instability can be considered using the Considère construction. In this approach the question of whether a polymer necks is answered by constructing a line on the true stress vs. draw ratio plot for the material from the origin to the stress–strain curve. If this line forms a tangent to the curve at any point necking will occur. Such a construction to the data for the fully relaxed material in Figure 10 reveals that the flow stress behavior of this grade of polyethylene is very close to that which might be shown by a material that does not neck. Consequently, small changes in the strain hardening may be sufficient to suppress necking, but the accuracy of the data

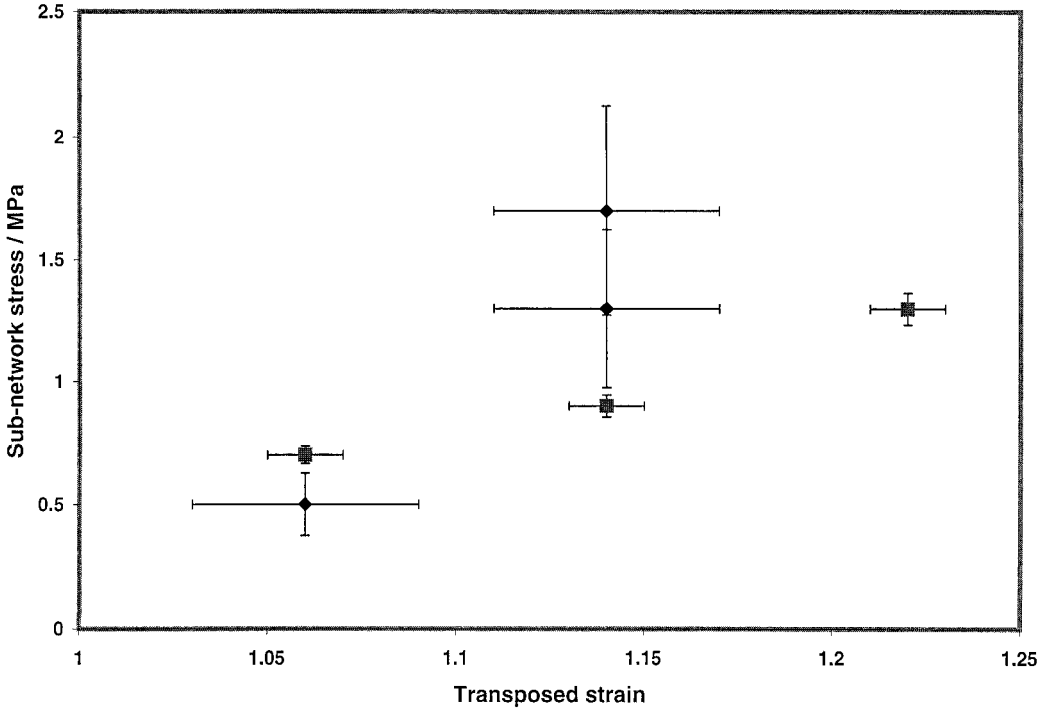

Figure 14 Comparison of the subnetwork stress in precursor sheets at an imposed draw ratio of 6 with the transposed strain λ_{res}, found in stress–strain curve matching. ■, center layer, ◆, surface layer.

presented here does not permit a detailed investigation. Nevertheless, this work shows that the absence or presence of necking correlates with the strain-hardening behavior at high strains. Where drawing occurs without the formation of a neck, higher strain hardening is observed. It has been shown above that the differences in strain-hardening behavior at high strains can be explained in terms of a molecular network formed during extrusion, which is retained during the subsequent drawing process. Although this subnetwork can make a detectable contribution at high deformations, it is quite surprising that it appears to play an important role at very low strains where necking occurs and where its contribution is very small.

CONCLUSIONS

The current work shows that the deformation behavior of a particular grade of high-density polyethylene varies significantly according to subtle differences in the nature of the starting material. It is observed that the presence or absence of necking correlates with the strain-hardening behavior at high strains. Where drawing occurs without the formation of a neck, higher strain hardening is observed. The differences in strain-hardening behavior at high strains can be explained in terms of a molecular network formed during extrusion, which is retained during the subsequent drawing process. The subnetwork characteristics vary depending on the level of extrusion and rate of cooling, with those entanglements surviving in the oriented melt at the point of crystallization having a long relaxation time. The impact of such small changes has particularly important implications for the processing industry, as there is the prospect of devising processing procedures that will remove or control the instability associated with necking.

References

1. Marshall, I.; Thompson, A. B. Proc R Soc 1954, 221, 541.
2. Vincent, P. I. Polymer 1960, 1, 7.
3. Mills, N. J. Br Polym J 1978, 10, 1.
4. Coates, P. D.; Ward, I. M. J Mater Sci 1980, 15, 2897.
5. Treloar, L. R. G. Physics of Rubber Elasticity; Clarendon Press: Oxford, 1975, 3rd ed.
6. Allison, S. W.; Pinnock, P. R.; Ward, I. M. Polymer 1966, 7, 6.
7. Ball, R. C.; Doi, M.; Edwards, S. F.; Warner, M. Polymer 1981, 22, 1010.
8. Edwards, S. F.; Vilgis, Th. Polymer 1986, 27, 483.
9. Long, S. D.; Ward, I. M. J Appl Polym Sci 1991, 42, 1921.
10. Sweeney, J.; Ward, I. M. Polymer 1995, 36, 299.
11. Buckley, C. P.; Jones, D. I. Polymer 1995, 36, 3301.
12. Capaccio, G.; Ward, I. M. Colloid Polym Sci 1982, 260, 46.
13. Brody, H. J Macromol Sci Phys 1983, B22, 407.
14. Long, S. D.; Ward, I. M. J Appl Polym Sci 1991, 42, 1911.
15. Osaki, K.; Nishizawa, K.; Kurata, M. Macromolecules 1982, 15, 1068.
16. Sweeney, J.; Caton-Rose, P.; Coates, P. D. Polymer, 2002, 43, 899.